Journal of
Ceramic Science
and Technology

J. Ceram. Sci. Technol., **13** [2] 113-120 (2022)
DOI: 10.4416/JCST2022-00007
available online at: http://www.ceramic-science.com
© 2022 Göller Verlag

Powder Modification Technology and Preparation of $MgAl_2O_4$ Transparent Ceramics by Hot Pressing

L. Guo[1], Y. Zhao[1], S. Xu[2], H. Shi*[1], A. Zheng[1], Y. Ma[1]

[1]GRINM Guojing Advanced Materials Co., Ltd., General Research Institute for Nonferrous Metals, Langfang 065001, PR China.
[2]Zhengzhou University, Zhengzhou 450000, PR China.

received June 12, 2022; received in revised form September 5, 2022; accepted October 17, 2022

Abstract

Hot-pressed $MgAl_2O_4$ transparent ceramics were successfully prepared based on powder modification technology using commercial $MgAl_2O_4$ powder. With a 2-wt% polyvinyl alcohol (PVA) addition and the powder modification treatment, the average particle size of the powder is 70 – 150 nm, the specific surface area is 32.16 m^2/g, and the median diameter (D (50)) is 7.2730 µm. Concluding the research about the effect of LiF on the properties of hot-pressed $MgAl_2O_4$ ceramics prepared based on powder modification technology, hot-press sintering proceeded well with a doping of 2 wt% PVA and 1 wt% LiF, and the mean maximum transmittance within the wave length range of 400 – 800 nm and 3 – 5 µm is 73.48 % and 83.09 % respectively, and the average grain size is 20 – 40 µm. XRD (X-ray diffraction) and ICP (Inductively Coupled Plasma) analysis of hot-pressed $MgAl_2O_4$ transparent ceramics indicate that the Li elements in hot-pressed transparent ceramics did not escape completely, but may exist as $LiAlO_2$.

Keywords: Powder modification technology, powder characterization, $MgAl_2O_4$ transparent ceramics, optical properties, hot pressing

I. Introduction

Spinel is a compound consisting of the AB_2O_4 isoaxial syngony composed of a group of molecules. In all spinel-like structures, the oxygen atoms form a cubic packing. In $MgAl_2O_4$, since the oxygen atoms are much larger than cations, Al^{3+} and $Mg^{2+}$are respectively inserted into the octahedral gap and tetrahedral gap formed by O^{2-} dense packing, and remain electrically neutral [1].

As an excellent mid-infrared material [2], $MgAl_2O_4$ transparent ceramics not only exhibit the properties of ceramic materials, such as high-temperature resistance, corrosion resistance, wear resistance, impact resistance, high hardness, high strength and good electrical insulation and so on [3–4], but also perform excellently in visible and infrared environments, Consequently, they are widely used in bulletproof windows, spacecraft protective windows and submarine infrared sensors and other military fields [5–6], as well as metal products of ceramic protective film, fine ceramic utensils and other civilian fields [7–9].

Although people have intermittently conducted research on $MgAl_2O_4$ transparent ceramics since the 1960s, it is still difficult to achieve low-cost sintering preparation of this material [10–13].

In order to commercialize the production of high-density, transparent and defect-free spinel products, people have repeatedly tried to develop economic and feasible production processes [14–19]. At present, it is difficult to form nano powders, which hinders the engineering application of $MgAl_2O_4$. In addition, mechanical mixing technology can also contaminate the powder. Even if the impurity content generated by the abrasion of the abrasive medium is very low, it can lead to opaque or fuzzy areas in the products [20]. However, it was found that the sintering additives and spinel powder were mixed unevenly before sintering, which was the main reason for the defects in these products. Currently, the traditional method of powder modification is achieved by some form of mechanical mixing of sintering auxiliary particles with spinel powder, for instance in a mortar and pestle, ball mill, grinder grinding or high shear wet grinding [21]. Moreover, A. Alhaji *et al.* proposed a plan to form a sintering additive coating on the spinel particles by dispersing the spinel particles in a liquor of sintering auxiliaries for spray drying [22]. While the spray drying method does achieve a more homogeneous distribution of sintering aids in spinel powders, this causes excessive loss of spinel powder, which means the yield after powder treatment does not exceed 68 %, so that more than 32 % of spinel powder treated by spray dryers will eventually be lost. Considering this low yield as well as the possible contamination during pumping of the solution, heating in the dryer, thermal air, and contact with the metal parts of the spray dryer during the spray drying process, this approach is not considered commercially attractive.

A relatively mature ceramic sintering process is hot-press sintering. This refers to a sintering method in which the dry powder is filled into the mould, and then pressed and heated from the uniaxial direction to complete moulding

* Corresponding author: shihc1977@126.com

and sintering at the same time. It can render the powder into a thermoplastic state with small deformation resistance, good plastic flow and high densification. In addition, since hot-press sintering is a sintering process with simultaneous heating and pressure, it aids the mass transfer processes such as contact, diffusion and flow of powder particles, reducing the sintering temperature and shortening the sintering time. At the same time, it is easy to obtain a sintered body with theoretical density and near-zero porosity by means of hot-press sintering, and realize crystal orientation. With the goal of preparing high-quality $MgAl_2O_4$ transparent ceramics by means of hot pressing, commercial $MgAl_2O_4$ powders are used raw material in the research detailed in this paper. Moreover, polyvinyl alcohol (PVA) binder was added in order to modify the powder to research the effects of PVA dosage on powder particle size, particle size distribution and specific surface area. At the same time, the performance of hot-pressed $MgAl_2O_4$ ceramics prepared with this powder modification technology was studied. The effect of different LiF content on the properties and micromorphology of hot-pressed $MgAl_2O_4$ was analysed. The content of Li in the transparent ceramics was measured, and the mechanism of LiF with regard to the sintering of hot-pressed spinel transparent ceramics was explained.

II. Experimental

(1) Materials and synthesis

0.5 wt% LiF + 1 wt% PVA, 1 wt% LiF + 2 wt% PVA, 1.5 wt% LiF + 3 wt% PVA, 2 wt% LiF + 4 wt% PVA (LiF purity ≥ 99.99 %, PVA purity ≥ 99.9 %) were added to four batches of commercial $MgAl_2O_4$ powder (purity ≥99.9 %) respectively, and recorded as 1#, 2#, 3#, 4#. First, Number 1# – 4# mixed powder, absolute ethanol dispersion and ZrO_2 material spheres (D15 mm, D1 mm, "D" representing the diameter of ZrO_2 sphere) were placed into an organic plastic container. Secondly, the container was placed in the three-dimensional mixer(the main function of this device was to thoroughly and evenly stir and mix the raw materials in the container) for 24 h (mixing frequency 50 Hz). Finally, the ZrO_2 balls were separated from the slurry in order to heat the slurry in a vacuum oven at 100 °C for 10 – 12 h, and then the dry paste was ground for 8 – 10 h into dried powder which needed to be sifted through a 40-mesh sieve. The treated powder (1#-4#) was filled into a graphite mould and sintered in HP-001 hot-press sintering equipment. First, the temperature was increased to 1 100 °C – 1 300 °C at a heating rate of 3 K/min – 15 K/min, and then the temperature was maintained at 1 000 °C – 1 100 °C for 60 min – 120 min. Secondly, the temperature was increased to 1 600 °C – 1 700 °C at the same rate and the pressure increased to 30 MPa – 50 MPa. Finally, the temperature and pressure were maintained for 4 – 6 h, and then the furnace was cooled down to obtain hot-pressed $MgAl_2O_4$ samples.

(2) Characterization methods

XRD analysis was performed on the commercial $MgAl_2O_4$ powder and the hot-pressed $MgAl_2O_4$ samples using an X-ray diffractometer (Rigaku, Japan) with CuK_α radiation ($\lambda = 1.5406$ Å) with a scan angle of 10 – 80° and a scan step size of 0.02 s; SEM/EDS analysis was conducted using a scanning electron microscope (Hitachi S-4800); TEM analysis was performed using a field emission transmission electron microscope (TECNAI G2 F20) operated at a voltage of 200 kV; The specific surface area of powder was measured with the BET method; The particle size of powder was analysed with a laser particle size analyzer (MYTOS-TWISTER); Infrared transmittance was measured at room temperature for polished samples (with a thickness of 4 mm) using a Fourier transform infrared (FTIR) spectrophotometer (Perkin Elmer LR-64912C) in the wavelength range of 3 – 5 μm. Visible spectra were recorded with a Shimadu UV-1900 spectrometer; The content of Li^+ in LiF-doped hot-pressed transparent ceramics was determined with the inductively coupled plasma (ICP) method.

III. Results and Discussion

(1) Effect of PVA on powder modification

Phase analysis of commercial raw materials was conducted and the result is shown in Fig. 1. The commercial $MgAl_2O_4$ powder XRD diagram is basically consistent with the standard card PDF #21 – 1152 diffraction peak, which is spinel phase with few impurity peaks. These impurities are usually Mg_2SO_4, α-Al_2O_3 and MgO, which is consistent with the result that the purity of high-purity powder is ≥ 99.9 % instead of 100 %. As introduced in other literature [23], one of the diffraction peaks of Mg_2SO_4 phase is $2\theta = 22.46$ °, and the other peaks with smaller intensity may be caused by the presence of α-Al_2O_3 and MgO.

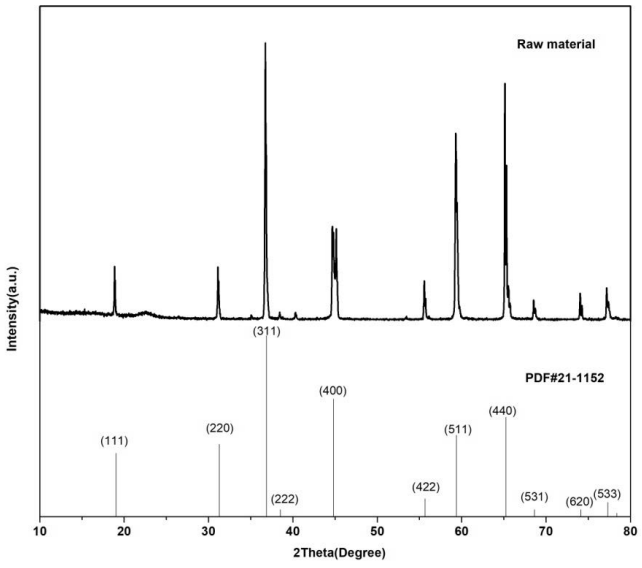

Fig. 1: Phase analysis of the commercial $MgAl_2O_4$ powder phase.

LiF is added to $MgAl_2O_4$ powder as a sintering aid, and LiF does not react with the powder during the powder modification process [24]. Owing to the small amount of LiF incorporated, the impact is on the particle size and granularity distribution of the powder can be ignored, to focus on the impact of PVA binder on powder modification. As shown in Fig. 2, the PVA doping mass ratio in 1# – 4#

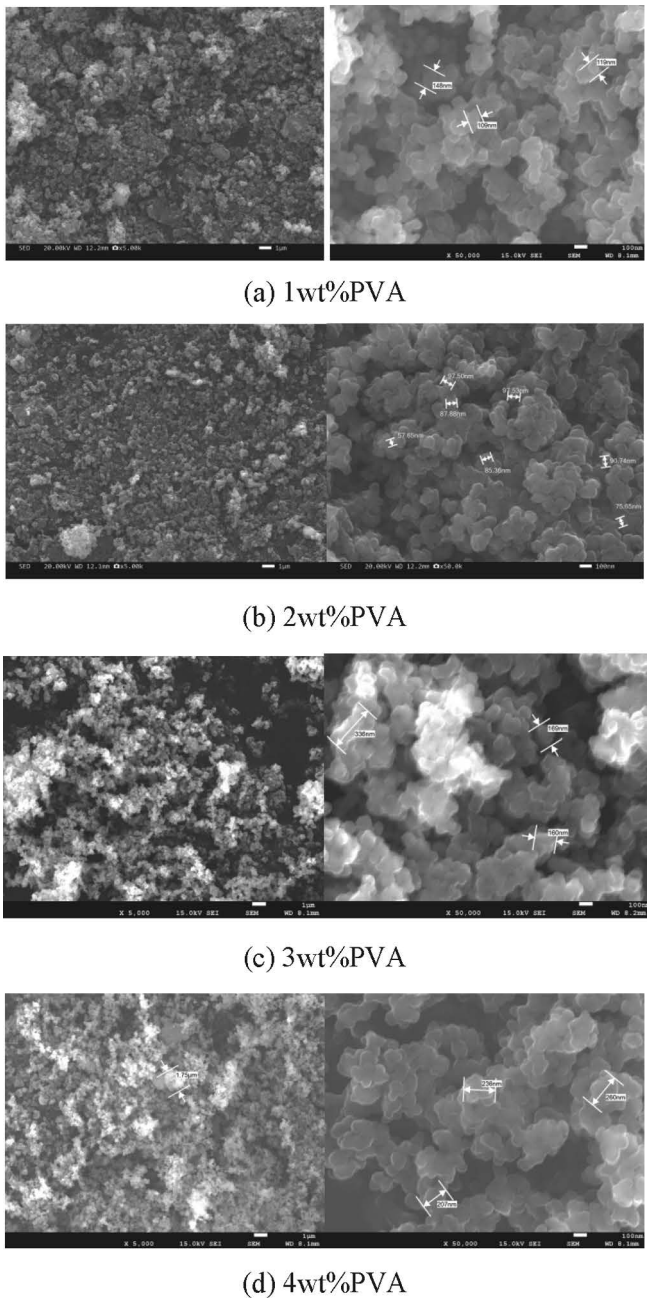

(a) 1wt%PVA

(b) 2wt%PVA

(c) 3wt%PVA

(d) 4wt%PVA

Fig. 2: SEM image of $MgAl_2O_4$ powder modified with the addition of a different content of PVA.

is 1 wt%, 2 wt%, 3 wt%, 4 wt%, and it was found that the powder particle disperses better when the amount of PVA doped is relatively low, which is shown in Fig. 2(a) and 2(b). As the amount of added PVA is increased, more agglomeration is detected, which is shown in Fig. 2(c) and 2(d). It can be seen from Fig. 2 that the particle size of sample 1# is 100 – 150 nm, for sample 2# it is 70 – 150 nm, for sample 3# it is 150 – 200 nm, and for sample 4# it is 200 – 260 nm. With the increase in PVA content, the particle size tends to increase. When the PVA content is 2 wt%, the powder particle size is smallest, which may be because PVA has the best wetting effect under this condition, prompting the powder to reach the best flow rate in the modification process. The TEM testing result for 1# – 4# powder samples is shown in Fig. 3. Significant agglomeration can be observed in Fig. 3(c) and 3(d). Compared with the condition when the mass ratio of added PVA is 3 wt% and 4 wt%, the agglomeration phenomenon is significantly less when the mass ratio of added PVA is 1 wt% and 2 wt%. The agglomeration observed in this TEM testing result is consistent with the SEM testing result. According to the BET test results, which are shown in Table 1, it can be seen that when the content of PVA is increased from 1 wt% to 4 wt%, the modified powder specific surface area is firstly increased from 25.68 m^2/g to 32.16 m^2/g and then reduced to 22.17 m^2/g. At this time PVA also wets the particles, prompting the generation of capillary force to adsorb particles. Therefore, the increase of added PVA leads to an increase of powder agglomeration and a decrease in specific surface area.

Table 1: Test results for specific surface area of powder obtained by modification treatment with different PVA content.

Sample number	1#	2#	3#	4#
Specific surface area (m^2/g)	25.68	32.16	23.97	22.17

The particle size of the treated powder (No.1#-4#) was analysed with a laser particle size analyzer. The granularity distribution diagram of modified $MgAl_2O_4$ powder with different amounts of added PVA is shown in Fig. 4. As the mass ratio of PVA increases from 1 wt% to 4 wt%, the median diameter (D50, "D50" can be understood as the corresponding particle size when the cumulative particle size distribution percentage of a sample reaches 50 %) of modified powder significantly increases from 5.7104 μm to 12.4053 μm, which is consistent with the theory that the more PVA is added, the more particles will ultimately combine with each other, so that the particle size tends to be enlarged.

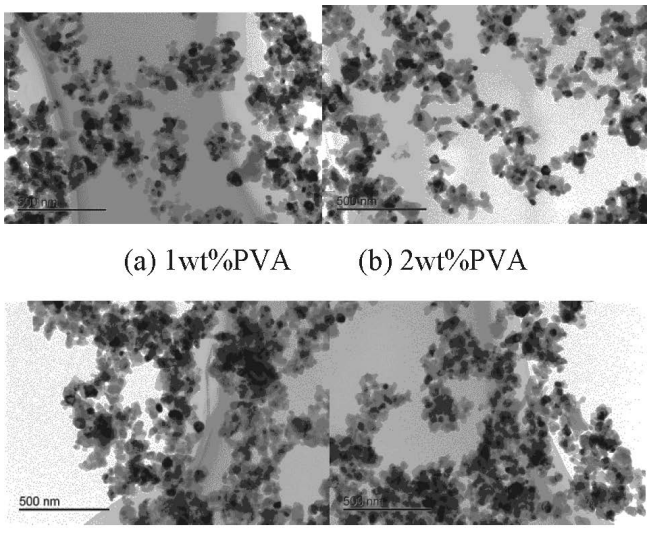

(a) 1wt%PVA (b) 2wt%PVA

(c) 3wt%PVA (d) 4wt%PVA

Fig. 3: TEM image of $MgAl_2O_4$ powder modified with a different content of PVA.

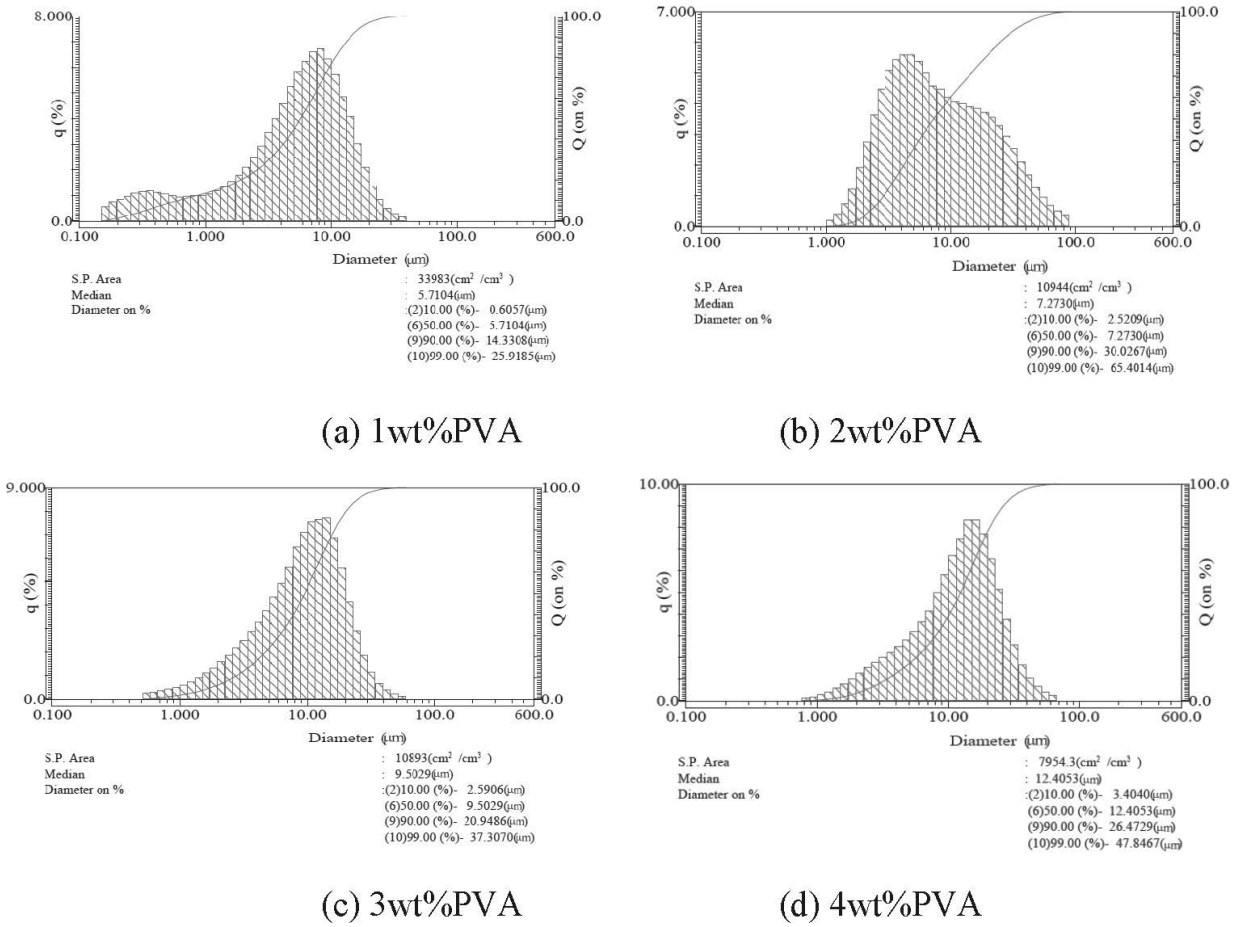

Fig. 4: Particle size distribution of $MgAl_2O_4$ powder modified with the addition of a different content of PVA.

(2) Effect of LiF on the properties and morphology of hot-pressed $MgAl_2O_4$ prepared based on powder modification

According to the hot-pressing process detailed in Section II (1), the modified 1# – 4# powder is hot-pressed, and the number of the hot-pressed $MgAl_2O_4$ sample corresponds to the modified powder sample number. As shown in Fig. 5, the mass ratio of LiF added to the hot-pressed sample number 1# – 4# is 0.5 wt%, 1 wt%, 1.5 wt%, 2 wt%, respectively. This clearly shows that increasing the doped amount of LiF enlarges the opaque fog-like region, and the reason for this phenomenon may be that the diameter of the internal scattering center of the material is in the order of the visible wavelength.

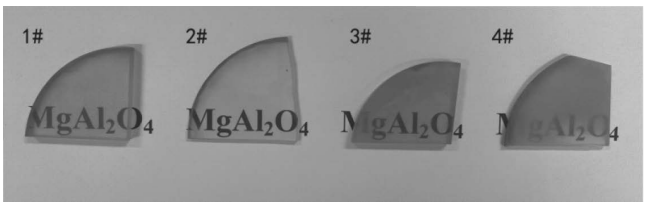

Fig. 5: Hot-pressed $MgAl_2O_4$ samples.

As shown in Fig. 6, the molar ratio of Al and Mg atoms in hot-pressed samples 1# – 4# calculated based on EDS data is close to 2:1, and the molar ratio of Al and Mg is shown in Table 2. No binder PVA component is found since PVA organic binder undergoes pyrolysis when heated to 200 °C. With consideration of the limitations of EDS quantitative analysis methods, the Li^+ content in the hot-pressed transparent ceramic after LiF doping was detected with the inductively coupled plasma (ICP) method, which is shown in Table 3. It can be seen from the detection results that the content of Li element in sample 1# is slightly higher than the content in the raw material powder, which may be caused by the uneven distribution of Li element in the sample, but the ICP detection results can still qualitatively evaluate the Li element content in the ceramic. The results in Table 3 show that the Li element content of the ceramic sample is reduced compared with the amount of LiF doped in the powder, indicating that there is a small amount of LiF escaping during the ceramic sintering process. This phenomenon is inconsistent with the statement described by Li *et al.* that LiF cannot escape in gaseous form [24], and is also inconsistent with the statement by Rozenburg *et al.* that LiF can be completely volatile [25]. According to the observation of the micromorphology of the hot-pressed sample 1# – 4#, as shown in Fig. 7, the average grain size of the hot-pressed sample 1# is 15 – 20 μm, for 2# it is 20 – 40 μm, for 3# it is 10 – 30 μm, and for 4# it is 10 – 30 μm. It can be seen clearly that there are more pores and agglomerated particles at the grain boundary after hot-press sintering. The position of the pores is marked with the red ellipse regions, and the particles agglomerated at the grain boundary are marked with the yellow rectangular areas, especially in the SEM images of hot-pressed samples 3# and 4#. In the SEM images of $MgAl_2O_4$

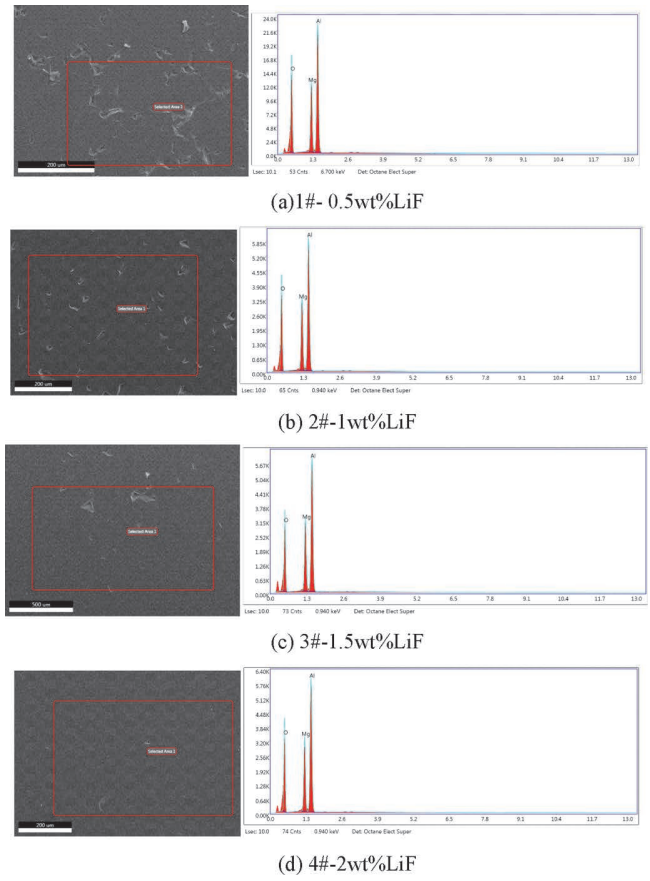

Fig. 6: EDS spectrum of $MgAl_2O_4$ transparent ceramic samples prepared by means of hot pressing with a different content of LiF.

ceramics prepared with the addition of different amounts of LiF, it can be seen that there are huge differences between the micromorphology of the hot-pressed samples prepared with different LiF doping amounts. When the LiF addition amount is 0.5 wt%, and 1 wt%, the grains grow when the $MgAl_2O_4$ powder is hot-pressed and sintered, but there is a small number of interconnected pores between the grains. When the mass ratio of LiF is 1.5 wt%, 2 wt%, it can be clearly seen from the SEM images in Fig. 7(a) and 7(b) that there are even more pores between the grains connected to each other. It can be seen from Fig. 7(a) – (b) that when the amount of LiF added is 1 wt%, the density of the 2# hot-pressed $MgAl_2O_4$ ceramic is higher and there are fewer pores than in the other samples. As described in other literature [23], although the hot-press sintering temperature and the amount of LiF doping are different from this experiment, the porosity phenomenon can also be explained on the basis of this principle: If hot-press sintering proceeds at relatively high temperature, LiF can be converted to a liquid state during the heating process and early sintering. Owing to the capillary force between the solid phase particles, the liquid phase tends to be inserted into the gap between solid particles, forming a liquid bridge between the solid-phase particles. In other words, at higher temperatures, the low-melting-point phase will migrate to the gap between the high-melting-point particles, leaving pores ($3LiF+MgAl_2O_4 \rightarrow Li_{Mg}' + 2Li_{Al}'' + 3F_O^{\cdot} + V_O^{\cdot\cdot}$) at its original position, which can effectively explain the pores observed in the SEM image in Fig. 7. It can be preliminarily inferred that low-melting-point material tends to lead to the formation of liquid phase during the ceramic sintering densification process, which promotes the densification process of the ceramic, but the aggregation of the liquid phase will lead to the formation of pores. A small amount of particle agglomeration at the grain boundaries can be clearly observed in Fig. 7, which may be caused when the $MgAl_2O_4$ powder in the hot-press sintering process reacts preferentially with the liquid phase LiF at high temperatures to form $LiAlO_2$ ($2LiF(v)+MgAl_2O_4(s) \rightarrow MgF_2(v)+2LiAlO_2(v)$), and another theory claims that the agglomerated particles leave a phase region rich in Mg or MgO [26], which may destroy the transparency, resulting in a dull colour of the sample. Although $2\theta = 77.46°$ shows simultaneously $LiAlO_2$ phase (L) and $MgAl_2O_4$ spinel phase (S) in Fig. 8(a) and 8(b), it can be inferred that the diffraction peak may be $LiAlO_2$ phase (L), which is consistent with the existence form of Li in ceramics measured by means of ICP.

Table 2: The molar ratio of Al and Mg in hot pressed samples 1#-4#.

Sample number	Preparation process	n(Al):n(Mg)
1#	HP	2.02
2#	HP	2.03
3#	HP	2.01
4#	HP	1.98

Table 3: Li_2O content in hot-pressed ceramic samples measured by ICP.

Sample number	Preparation process	LiF addition [wt%]	Li_2O detected [wt%]	Equivalent LiF concentration [wt%]
1#	HP	0.5	0.31	0.54
2#	HP	1	0.56	0.98
3#	HP	1.5	0.71	1.23
4#	HP	2	1.06	1.84

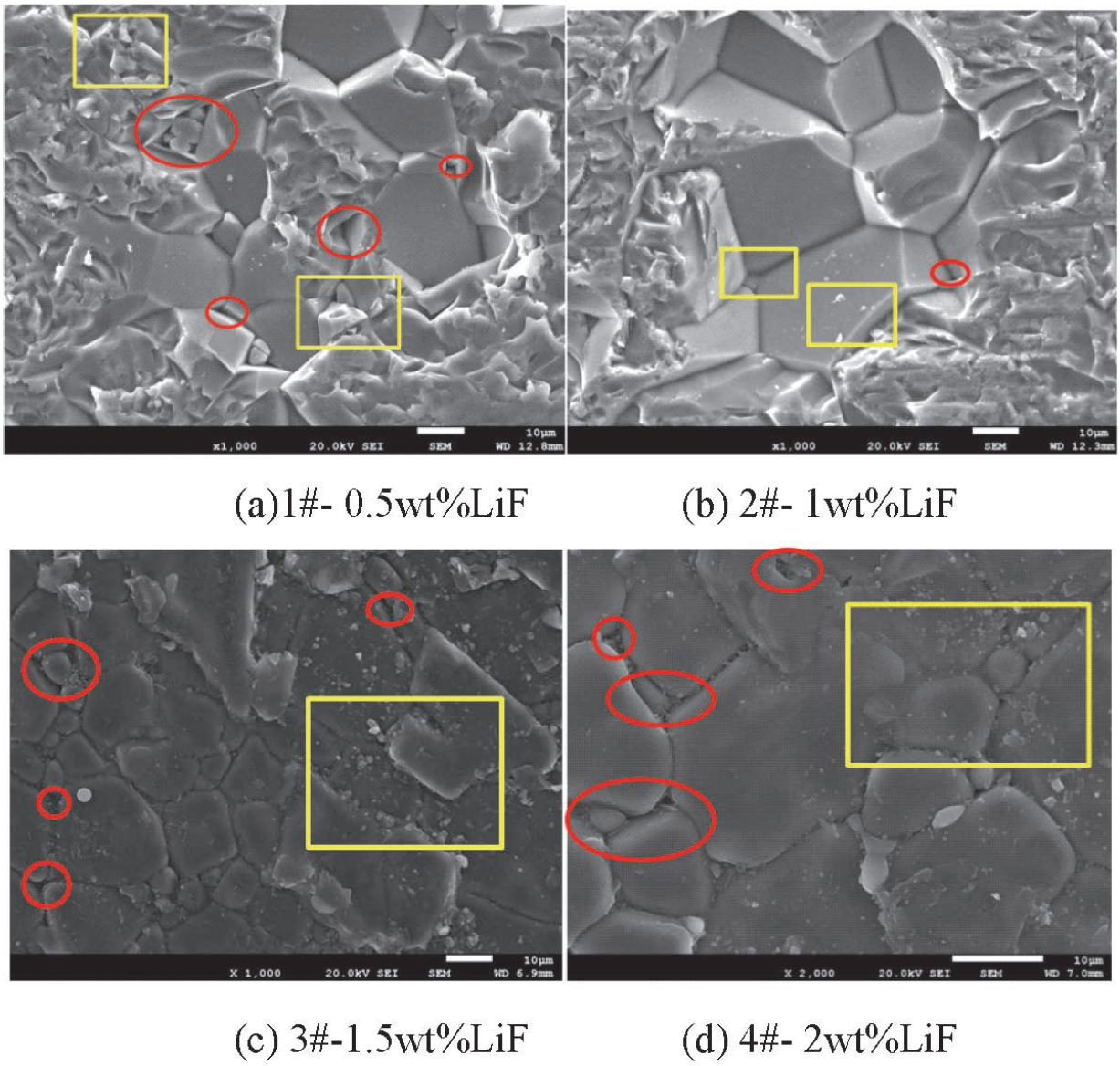

Fig. 7: SEM images of $MgAl_2O_4$ transparent ceramic samples prepared by means of hot pressing with a different content of LiF.

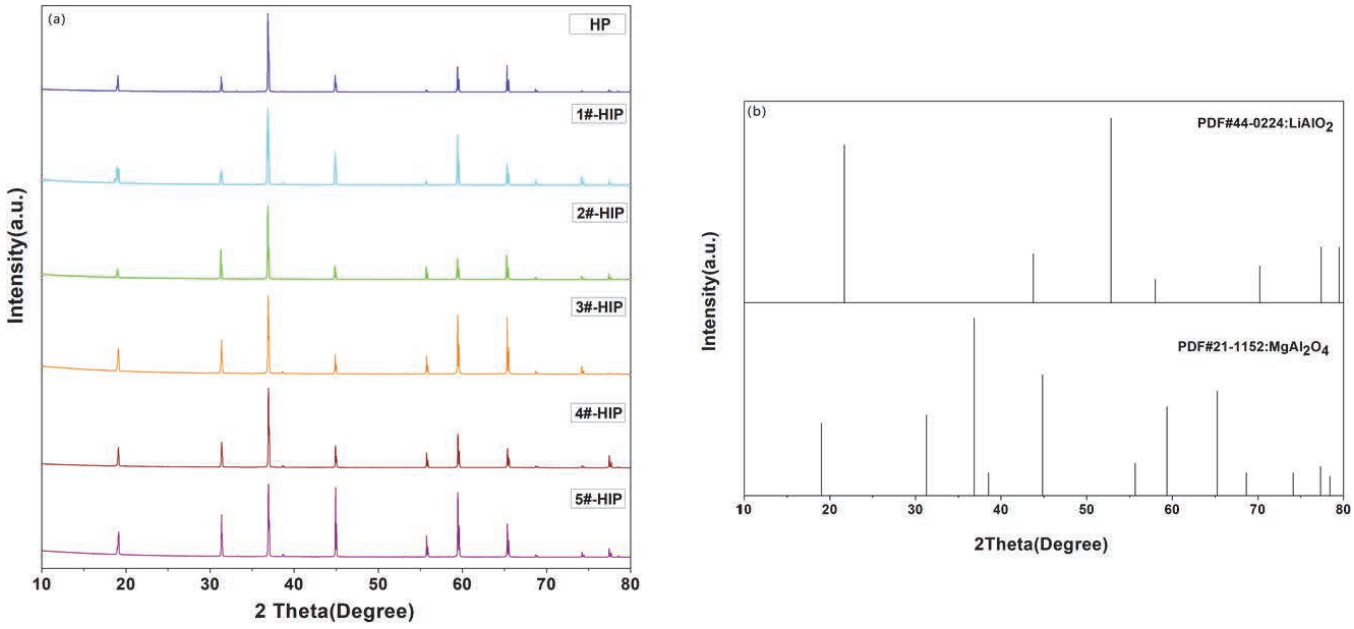

Fig. 8: XRD pattern, (a) Hot-pressed sample 1#-4# XRD pattern, (b) PDF card of $MgAl_2O_4$ spinel phase (s) and $LiAlO_2$ (L) phase.

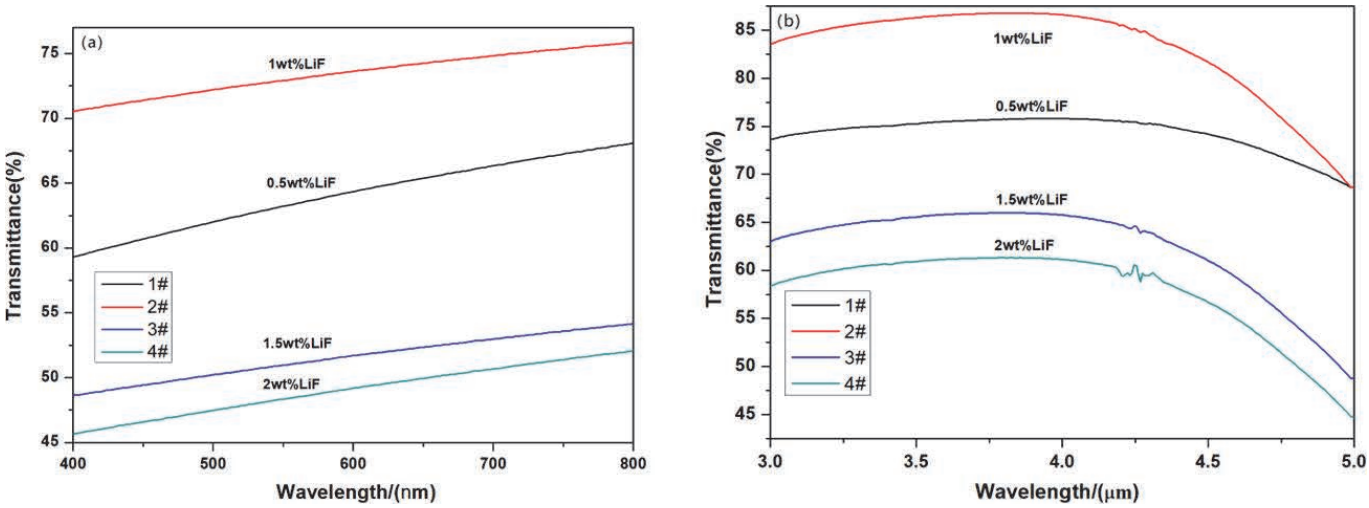

Fig. 9: Optical transmission curve of hot-pressed $MgAl_2O_4$ transparent ceramics with a different LiF content. The sample thickness is 4 mm, (a) transmission curve of 400 nm – 800 nm, (b) 3 μm – 5 μm transmission curve.

The MgO phase is not discovered owing to the problem of dispersion uniformity of the LiF sintering aid during the previous powder modification treatment. As Belov [27] described [27], Li^+ can replace Mg in spinel, F^- can replace lattice bits of oxygen. This produces $LiAl_2(O_{0.75}, F_{0.25})_4$, which means some Mg or Li moves to the Al position, forming an inverted spinel structure and oxygen vacancies, thus leading to the generation of phases rich in Mg or MgO as well as oxygen vacancies.

Fig. 9 shows the optical transmission curve of the hot-pressed $MgAl_2O_4$ transparent ceramic with different LiF content. Fig. 9(a) indicates that after hot-press sintering, with the increasing amount of added LiF, the phenomenon of firstly increasing and then decreasing in the 400 – 800 nm range is shown, and when the mass ratio of added LiF is 1 wt%, the average optical transmittance in the range of 400 – 800 nm is the maximum value; the optical transmittance of hot-pressed sample 2# is 73.48 %, and that of the other hot-pressed samples 1#, 3#, #4 is 64.12 %, 51.57 % and 49.06 %, respectively. Similarly, the transmission curve also appeared to firstly increase and then decrease in the range of 3 – 5 μm. When the mass ratio of added LiF is 1 wt%, the average optical transmittance reaches the maximum value, while the transmittance of hot-pressed sample 2# is 83.09 %, and the average transmittance of the other hot-pressed samples 1#, 3#, and 4# at the wavelength range of 3 – 5 μm is 74.32 %, 62.46 % and 57.98 %, respectively. With the increase of added LiF, the transmittance of hot-pressed samples 1# – 4# at 400 – 800 nm and 3 – 5 μm has firstly increased and then decreased, and the opacity of hot-pressed samples 3# and 4# can be clearly observed from the hot-pressed samples in Fig. 5. Combined with the SEM image of the hot-pressed samples in Fig. 7 and the XRD analysis of the hot-pressed samples in Fig. 8, it is preliminarily inferred that this is due to the optical scattering caused by the pores at the grain boundaries and the second phase of $LiAlO_2$. At the same time, the low average transmittance of 400 – 800 nm may be caused by the light scattering of residual pores and agglomeration of small particles at the grain boundary. The pore size is close to the incident wavelength, resulting in Mie scattering [28], which is shown in Figs. 7(c) and 7(d).

IV. Conclusions

This paper discusses the effect of adding different dosages of PVA binder on the particle size, granularity and specific surface area of powder. Based on analysis of the SEM and TEM images of the treated powder, it is found that adding an appropriate amount of PVA is conducive to the powder achieving the best wetting effect, reducing the average particle size of the powder, improving the specific surface area of the powder, and promoting the dispersibility of the powder granularity. When the amount of added PVA is 2 wt%, the average particle size of the powder is 70 – 150 nm, the specific surface area is 32.16 m^2/g and the D(50) is 7.2730 μm after the powder modification treatment. Moreover, the effect of LiF on the properties of hot-pressed $MgAl_2O_4$ ceramics prepared based on powder modification technology was studied, which indicated that 2 wt% added PVA and 1 wt% sintering auxiliary LiF is the best recipe to promote hot-press sintering. With this recipe, the average transmittance in the bands of 400 – 800 nm and 3 – 5 μm is 73.48 % and 83.09 %, respectively, and the average grain size is 20 – 40 μm. XRD pattern and ICP test analysis indicated that Li element in the hot-pressed transparent ceramic did not completely escape, but may exist as $LiAlO_2$. Combined with the properties of the hot-pressed sample and the analysis of the average transmission curve in the range of 400 – 800 nm and 3 – 5 μm, the addition of excess LiF will reduce the average transmittance in the range of 400 – 800 nm and 3 – 5 μm, resulting in white flocs inside the hot-pressed ceramics.

Acknowledgements

This work was supported by General Research Institute for Nonferrous Metals Innovation Fund (No. 2020TS0204), GRINM Advanced Materials Co., Ltd. Innovation Fund (No. G2021KC0202).

References

1 Huaizhi, Y.: Infrared optical materials, Second Edition [M] Beijing: National Defense Industry Press, 72 – 73, (2015).

2 Shi, Z., Zhao, Q., Guo, B., *et al.*: A review on processing polycrystalline magnesium aluminate spinel ($MgAl_2O_4$): Sintering techniques, material properties and machinability, *Mater. Design*, 193:108858(2020). doi: https://doi.org/10.1016/j.matdes.2020.108858.

3 Harris, D.C.: History of development of polycrystalline optical spinel in the U.S., Proc. SPIE – Int. Soc. Opt. Eng., 1 – 22, (2005). doi: https://doi.org/10.1117/12.609708.

4 Sepulveda, J.L., Loutfy, R.O., Ibrahim, S., *et al.*: Large-size spinel windows and domes[C]//Window & Dome Technologies & Materials XIII, Int. Soc. Opt. Photon., 2013. doi: https://doi.org/10.1117/12.2016442.

5 Mroz, T.J., Hartnett, T.M., Wahl, J.M., *et al.*: Recent advances in spinel optical ceramic, *Proc Spie*, 5786, (2005). doi: https://doi.org/10.1117/12.607593.

6 Gilde, G., Patel, P., Sands, J., Patterson, P., *et al.*: Evaluation of hot isostatic pressing parameters on the optical and ballistic properties of spinel for transparent armor, *J. Am. Ceram. Soc.*, **88**, [10], 2747 – 51, (2006).

7 Rubat du Merac, M., Kleebe, H.J., Müller, M.M., Reimanis, I.E.: Fifty years of research and development coming to fruition; Unraveling the complex interactions during processing of transparent magnesium aluminate ($MgAl_2O_4$) spinel, *J. Am. Ceram. Soc.*, **96**, 3341 – 3365, (2013). doi: https://doi.org/10.1111/jace.12637.

8 Baudin, C., Pena, P.: Influence of stoichiometry on fracture behavior of magnesium aluminate spinels at 1 200 °C, *J. Eur. Ceram. Soc.*, **17**, 1501 – 11 (1997).

9 Jiang, L.P., Jiang, X. *et al.*: Multiobjective machine learning-assisted discovery of a novel cyan-green garnet: Ce phosphors with excellent thermal stability, *ACS Appl. Mater. Inter.*, **14**, [13], 15426 – 15436, (2022). doi: https://doi.org/10.1021/acsami.2c02698.

10 Bratton, R.J.: Translucent sintered $MgAl_2O_4$, *J. Am. Ceram. Soc.*, **57**, [7], 283 – 6, (1974). doi: https://doi.org/10.1111/j.1151 – 2916.1974.tb10901.x.

11 Hing, P.: Fabrication of Translucent Magnesium aluminate spinel and its compatibility in sodium vapour, *J. Mater. Sci.*, **11**, 1919 – 26, (1976). doi: https://doi.org/10.1007/BF00708270.

12 Benameur, N., Bernard-Granger, G., *et al.*: Sintering analysis of a fine-grained alumina-magnesia spinel powder, *J. Am. Ceram. Soc.*, **94**, [5], 1388 – 96 (2011). doi: https://doi.org/10.1111/j.1551 – 2916.2010.04271.x.

13 Morita, K., Kim, B.-N., Hiraga, K., Yoshida, H.: Fabrication of transparent $MgAl_2O_4$ spinel polycrystal by spark plasma sintering process, *Scripta Mater.*, **58**, 1114 – 7, (2008). doi: https://doi.org/10.1016/j.scriptamat.2008.02.008

14 Meir, S., Kalabukhov, S., *et al.*: Synthesis and densification of transparent magnesium aluminate spinel by sps processing, *J. Am. Ceram. Soc.*, **2**, 358 – 64, (2009). doi: https://doi.org/10.1111/j.1551 – 2916.2008.02893.x

15 Bonnefont, G., Fantozzi, G., *et al.*: Fine-grained transparent $MgAl_2O_4$ spinel obtained by spark plasma sintering of commercially available nanopowders, *Ceram. Int.*, **38**, 131 – 41, (2012). doi: https://doi.org/10.1016/j.ceramint.2011.06.045.

16 Liu, G., Li, J., Yang, Z.: Melt-casting of translucent $MgAl_2O_4$ ceramics by combustion synthesis under high gravity, *Mater. Manuf. Process.*, **27**, [6], 689 – 93, (2012). doi: https://doi.org/10.1080/10426914.2011.593250.

17 Mazzoni, A.D., Sainz, M.A., *et al.*: Formation and sintering of spinels ($MgAl_2O_4$) in reducing atmospheres, *Mater. Chem. Phys.*, **78**, 30 – 7, (2002). doi: https://doi.org/10.1016/S0254 – 0584(02)00333 – 4.

18 Esposito, L., *et al.*: Production and characterization of transparent $MgAl_2O_4$ prepared by hot pressing, *J. Eur. Ceram. Soc.*, **33**, 737 – 47, (2013). doi: https://doi.org/10.1016/j.jeurceramsoc.2012.10.013.

19 Lei, M-Y., Huang, C.-X., Sun, J.-L.: Effect of HIP on the properties and microstructure of transparent polycrystalline spinel, *Key Eng. Mat.*, **336 – 338**, 1200 – 2 (2007).

20 Villalobos, G.R., Sanghera, J.S., Aggarwal, I.D.: Degradation of magnesium aluminum spinel by lithium fluoride sintering aid, *J. Am. Ceram. Soc.*, **88**, [5], 1321 – 1322, (2010). doi: https://doi.org/10.1111/j.1551 – 2916.2005.00209.x.

21 Liu, Q., Jing, Y., Su, S., *et al.*: Microstructure and properties of $MgAl_2O_4$ transparent ceramics fabricated by hot isostatic pressing, *Opt. Mater.*, **104**, (2020). doi: https://doi.org/10.1016/j.optmat.2020.109938

22 Alhaji, A., Taherian, M.H., Ghorbani, S., *et al.*: Development of synthesis and granulation process of $MgAl_2O_4$ powder for the fabrication of transparent ceramic, *Opt. Mater.*, 98:109440(2019). doi: https://doi.org/10.1016/j.optmat.2019.109440.

23 Zhou, Y., Ye, D., Wu, Y. *et al.*: Low-cost preparation and characterization of $MgAl_2O_4$ ceramics, *Ceram. Int.,* **48**, [5], 7316 – 7319, (2022). doi: https://doi.org/10.1016/j.ceramint.2021.11.196.

24 Fa Hui, L.I., Lin, H., Junfeng L.I., *et al.*: Influence of LiF on the infrared transmissivity of magnesia alumina spinel transparent ceramics, *J. Inorg. Mater.*, **27**, [4] 417 – 421, (2012). doi: https://doi.org/10.3724/SP.J.1077.2012.00417

25 Rozenburg, K., Reimanis, I.E., Kleebe, H.J., *et al.*: Chemical interaction between LiF and $MgAl_2O_4$ spinel during sintering, *J. Am. Ceram. Soc.*, **90**, [7], 2038 – 2042, (2007). doi: https://doi.org/10.1111/j.1551 – 2916.2007.01723.x

26 Sutorik, A.C., Gilde, G., Cooper, C., Wright, J., Hilton, C.: The effect of varied amounts of lif sintering aid on the transparency of alumina rich spinel ceramic with the composition $MgO\text{-}1.5Al_2O_3$, *J. Am. Ceram. Soc.*, **95**, [6], 1807 – 10, (2012). doi: https://doi.org/10.1111/j.1551 – 2916.2012.05217.x

27 Belov, S.F., Adaeva, T.I., Rozdin, I.A., Varfolomeev, M.B.: Reaction of Al_2O_3 with LiF, *Refractories*, **26**, 1675 – 6, (1985).

28 Li, X.Y., Liu, Q., Hu, Z.W., Jiang, N., Shi, Y., Li, J.: Influence of ammonium hydrogen carbonate to metal ions molar ratio on co-precipitated nanopowders for TGG transparent ceramics, *J. Inorg. Mater.*, **34**, 791 – 796, (2019). doi: https://doi.org/10.15541/jim20180574.